ISSN 1063-7834, Physics of the Solid State, 2007, Vol. 49, No. 6, pp. 1116–1120. © Pleiades Publishing, Ltd., 2007.
Original Russian Text © S.G. Ovchinnikov, B.A. Gizhevskiĭ, Yu.P. Sukhorukov, A.E. Ermakov, M.A. Uĭmin, E.A. Kozlov, Ya.A. Kotov, A.V. Bagazeev, 2007, published in Fizika Tverdogo Tela, 2007, Vol. 49, No. 6, pp. 1061–1065.

OPTICAL PROPERTIES

Specific Features of the Electronic Structure and Optical Spectra of Nanoparticles with Strong Electron Correlations

S. G. Ovchinnikov[a], B. A. Gizhevskiĭ[b], Yu. P. Sukhorukov[b], A. E. Ermakov[b], M. A. Uĭmin[b], E. A. Kozlov[c], Ya. A. Kotov[d], and A. V. Bagazeev[d]

[a] *Kirensky Institute of Physics, Siberian Division, Russian Academy of Sciences, Akademgorodok, Krasnoyarsk, 660036 Russia*

[b] *Institute of Metal Physics, Ural Division, Russian Academy of Sciences, ul. S. Kovalevskoĭ 18, Yekaterinburg, 620041 Russia*

e-mail: gizhevskii@imp.uran.ru

[c] *Russian Federal Nuclear Center, Zababakhin All-Russia Research Institute of Technical Physics, Snezhinsk, Chelyabinsk oblast, 456770 Russia*

[d] *Institute of Electrophysics, Ural Division, Russian Academy of Sciences, ul. Amundsena 106, Yekaterinburg, 620016 Russia*

Received September 14, 2006

Abstract—Analysis of the experimental optical spectra of CuO nanoparticles with the electronic structure characterized by strong electron correlations has revealed the appearance of unusual states inside the band gap. The intragap states and the specific features of the electronic structure of CuO nanoparticles are discussed in the framework of the generalized tight-binding method previously developed for describing the electronic structure of superconducting cuprates.

PACS numbers: 74.72.-h, 74.20.-z

DOI: 10.1134/S1063783407060169

1. INTRODUCTION

It is natural to expect that the changeover from classical bulk semiconductors and insulators to nanoparticles should be accompanied by a broadening of the band gap and, hence, a blue shift in the fundamental absorption edge. This effect is well described in the framework of the simplest one-electron band model as a consequence of the quantum confinement [1]. In particular, the corresponding effect has been observed for the Cu_2O semiconductor, whose electronic structure is adequately described within the band theory [1]. A different behavior has been revealed for nanoparticles of materials with strong electron correlations, such as copper monoxide CuO. In this case, the changeover from bulk materials to nanoparticles leads to a noticeable red shift [2]. In the present paper, we generalize the experimental data on the optical absorption spectra of CuO nanoparticles prepared by different methods and discus the results in terms of the many-electron approach developed earlier for describing high-temperature superconducting cuprates [3]. For doped compounds with strong electron correlations, this approach predicts the appearance of intragap levels with a high density of states and, hence, an optical density at energies lower than the energy E_g corresponding to the fundamental absorption edge.

2. SPECIFIC FEATURES OF THE OPTICAL PROPERTIES OF CuO NANOPARTICLES

The measurement of optical absorption spectra of semiconductors is the direct and most reliable method for determining the fundamental absorption edge (i.e., the energy E_g, which corresponds to the band gap) and the specific features of the electronic structure at energies of electronic transitions in the IR, visible, and UV spectral ranges (<6 eV). In order to verify the assumptions regarding the appearance of intragap states and the specific features of the electronic structure of nanooxides with strong electron correlations, we investigated the absorption spectra for a number of samples of nanostructured oxide CuO. Copper monoxide is an antiferromagnet with strong electron correlations and a band gap of 1.45 eV [4]. The optical properties of the CuO oxide are strongly affected by the type and concentration of defects in the sample. In order to reveal the effects associated with the nonstoichiometry and the defect structure, we studied samples of nanostructured oxide CuO that consisted of microcrystallites approximately identical in size but were prepared using different methods. The concentration and type of defects depend substantially on the preparation technique. In our samples, the crystallite sizes were less than 50 nm. As was shown in our previous works, the specific features of the nanostructured state and optical properties of copper oxides, such as the red shift of the

absorption edge for the CuO oxide and the blue shift for the Cu_2O oxide, begin to manifest themselves at these crystallite sizes [2].

The optical investigations were performed with CuO high-density nanoceramics and CuO nanopowders. The nanoceramic materials were prepared from a coarse-grained polycrystalline CuO by loading with converging spherical shock waves [5, 6]. The nanopowders were produced by the gas-phase method via condensing copper vapors in an argon medium containing oxygen and by electric explosion of a copper wire in a nitrogen–oxygen mixture [7, 8]. The samples were characterized by x-ray diffraction, and a number of samples were examined using scanning electron microscopy (SEM) and scanning tunneling microscopy (STM). The sizes of crystallites (coherent scattering regions) and the microstrains were evaluated from the broadening of x-ray diffraction lines. The estimated crystallite sizes are in agreement with the SEM and STM data. The analysis of the x-ray powder diffraction data demonstrated that the CuO nanoceramic materials have a single-phase composition and a monoclinic lattice with parameters close to those of the equilibrium copper oxide. The CuO nanopowders contained the Cu_2O phase in amounts up to 18%. The samples prepared by the aforementioned three methods and having close crystallite sizes (15–40 nm) were chosen for optical measurements.

The spectral dependences of the optical density $D = \ln 1/T$ (where T is the transmittance) were studied for the copper oxide nanopowders because of the very strong absorption and the uncertainty in the estimate of the sample thickness. The transmittance spectra were measured in the range 0.2–3.5 eV at room temperature on spectrometers operating in the IR and visible ranges with a transmittance sensitivity of $\sim 10^{-4}$. The nanoceramic samples for the absorption measurements were prepared by mechanical polishing in the form of plates 40–60 μm thick. In the case of nanopowders, the samples were produced directly during the preparation of the nanomaterials by evaporating the nanopowders on glass and quartz substrates. The measured spectra were compared with those of CuO and Cu_2O single crystals (Fig. 1). The presence of some amount of the Cu_2O phase in the nanopowders does not substantially affect the spectrum of the main material, because the fundamental absorption edge of the Cu_2O oxide is located at 2.1 eV and only weak absorption bands at energies of 0.14 and 0.10 eV are observed in the transparency window of this oxide.

Nanostructured oxides are nonequilibrium materials with a considerable concentration of point and surface defects. The high concentration of oxygen vacancies in CuO nanoceramic materials can be judged from the experimental data on angular correlations of annihilation radiation [9]. Druzhkov et al. [9] showed that oxygen vacancies and their small-sized clusters are predominantly located at crystallite boundaries and their

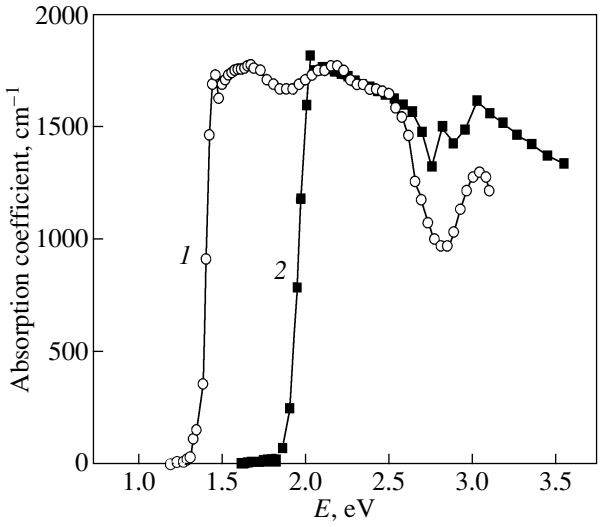

Fig. 1. Absorption spectra of (*1*) CuO and (*2*) Cu_2O single crystals.

concentration decreases with an increase in the crystallite sizes. The concentration of cations with a decreased valence was estimated using x-ray photoelectron spectroscopy [10]. Note that single-phase samples, according to the x-ray diffraction data contained up to 8–10% Cu^+. These high defect concentrations cannot be observed in equilibrium polycrystalline or single-crystal CuO samples. The ratios between the copper and oxygen concentrations measured by the nuclear-reaction method and Rutherford backscattering indicate a considerable disturbance of the stoichiometry of CuO nanomaterials [11]. Therefore, the inference can be made that oxygen vacancies and cations with a decreased valence in the form of individual point defects or their clusters are the main types of defects in copper nanooxides.

The absorption spectra of all copper nanooxide samples are characterized by a strong smearing of the fundamental absorption edge and a shift of the optical density toward low energies. This suggests that levels with a high density of states appear in the band gap. The appearance of intragap states leads to a decrease in the effective band gap. The effective band gap estimated for the copper nanooxide samples from the transparency window decreases to 0.7–0.5 eV, whereas the band gap for CuO single crystals is equal to 1.45 eV [4]. Against the background of a relatively monotonic decrease in the optical density with a decrease in the energy below ~1.5 eV, there are specific features that can be characterized as individual broad absorption bands. In particular, the broad "impurity" band at ~0.6 eV is clearly seen for the nanopowder prepared by the gas-condensation method (Fig. 2, curve *2*). For the nanoceramic sample and the nanopowder produced by electric explosion, the spectral dependences of the optical density exhibit kinks at energies of ~1.3 and

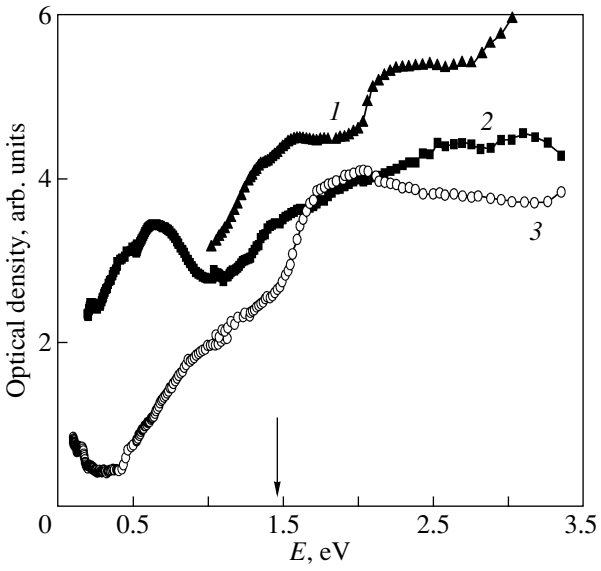

Fig. 2. Absorption spectra of CuO nanooxides: (*1*) the nanoceramic material, (*2*) the nanopowder prepared through gas condensation, and (*3*) the nanopowder produced by electric explosion. The arrow indicates the fundamental absorption edge of the CuO single crystal.

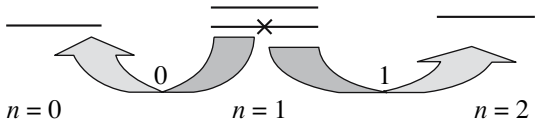

Fig. 3. Schematic diagram of the many-electron levels in different subspaces of the Hilbertian space for the numbers of holes 0, 1, and 2 per unit cell. The cross indicates the spin level filled at $T = 0$ for the stoichiometric oxide CuO. Arrows with numerals 0 and 1 identify one-electron quasiparticles corresponding to the bottom of the conduction band and the top of the valence band.

~1.0 eV, respectively (Fig. 2). It should be noted that similar absorption bands at energies of 0.8–1.0 eV were observed for CuO single crystals irradiated by electrons and He^+ ions [12, 13]. The appearance of these bands was attributed to the formation of Cu^+ ions and their clusters. The difference in the location of the impurity bands can be associated both with the difference in the concentration of impurities and defects in different samples and with the difference in the type of defects. For example, there can arise small-sized clusters composed of oxygen vacancies ("pairs," "triads," etc.) and complexes in the composition of oxygen vacancies and Cu^+ ions. The contribution to the smearing of the fundamental absorption edge is also made by the microstrains, which, in the nanoceramic material, can be as large as 0.5% [6]. In our opinion, in all cases, the appearance of intragap states and the corresponding red shift in the absorption edge for nanostructured copper oxides are associated with the high concentration of nonstoichiometric defects and the specific features of the electronic structure of oxides with strong electron correlations.

3. SPECIFIC FEATURES OF THE ELECTRONIC STATE AND INTRAGAP STATES FOR CuO NANOPARTICLES

One of the main experimental findings is the increase in the number of oxygen vacancies and the concentration of Cu^+ ions in nanoparticles as compared to bulk copper monooxide samples. From the standpoint of the electronic structure of Mott–Hubbard insulators, including copper monooxide, the same defects are responsible for electron doping. As in layered high-temperature superconducting cuprates, the doping results in the appearance of intragap states. Let us consider the mechanism of their formation in more detail as applied to copper monooxide.

In view of strong electron correlations, the electronic structure of the CuO oxide will be discussed in the framework of the generalized tight-binding method, which was specially developed for systems with strong electron correlations [3]. At the first stage of the generalized tight-binding method, the exact diagonalization is performed for a many-electron cluster simulating a unit cell. At the second stage, jumps that occur between many-electron terms of neighboring unit cells and lead to their dispersion and the formation of a band structure are taken into account within the perturbation theory. The unit cell can be represented by a CuO_4 cluster. Owing to the electroneutrality of the crystal, the following valences can be assigned to the ions in the stoichiometric case: $Cu^{2+}O_4^{2-}$. The many-electron terms of the unit cell will be numbered according to the number of holes. In particular, for the $3d^92p^6$ configuration, we have one hole per unit cell ($n_h = 1$). The addition of one electron leads to the formation of the $3d^{10}2p^6$ configuration with $n_h = 0$ (or Cu^+). The addition of one hole results in the formation of two-hole terms with $n_h = 2$, which are described by the superposition of the $3d^82p^6$, $3d^92p^5$, $3d^{10}2p^52p^5$, and $3d^{10}2p^4$ configurations (with a finite probability, there appear Cu^{3+} ions).

The same CuO_4 cluster was considered within the generalized tight-binding method when calculating the electronic structure of the n-Nd_2CuO_4 high-temperature superconductor [14]. Figure 3 schematically depicts three orthogonal subspaces of the Hilbertian space with the numbers of holes $n_h = 0$ (n_0), 1 (n_1), and 2 (n_2) and the many-electron terms E_0 ($S = 0$), $E_{1\sigma}$ ($S = 1/2$, $\sigma = \pm 1/2$), and E_2 ($S = 0$). The spin doublet $E_{1\sigma}$ is split by the internal two-sublattice molecular field. The cross indicates the spin sublevel filled at $T = 0$. The arrows show the one-particle Fermi excitations: the addition of one electron (the band index 0 corresponds to the bottom of the empty conduction band $\Omega_\sigma^{(c)} = E_\sigma - E_0$) and the addition of one hole (the band index 1

corresponds to the top of the valence band $\Omega_\sigma^{(v)} = E_2 - E_{1,\bar{\sigma}}$). Here, we have $\bar{\sigma} = -\sigma$. The band gap between the filled band and the empty conduction band (in the given case, the charge-transfer band gap) amounts to $E_{g0} = \Omega^{(c)} - \Omega^{(v)} = 2E_{1\sigma} - E_0 - E_2$ at typical parameters for cuprates $E_{g0} \approx 2$ eV. The difference between the Nd_2CuO_4 and CuO compounds from the viewpoint of their electronic structures lies only in the type of three-dimensional packing of unit cells. This eventually manifests itself in the difference between the dispersion laws for electronic quasiparticles in the vicinity of the top of the filled valence band and the bottom of the empty conduction band. However, the dispersion is small (with a typical width of approximately 0.3–0.4 eV). Therefore, the difference between the types of unit cell packing in the structures of the CuO and Nd_2CuO_4 compounds can lead to a change of the order of 0.1 eV in the band gap.

The physical mechanism of formation of new intragap states upon both *n*- and *p*-type doping can be easily explained using Fig. 4. The electron doping (it is assumed that x is the concentration of Cu^+ ions) leads to a change in the occupation number of the terms shown in Fig. 3 (they are determined by solving the self-consistency equation for the chemical potential). At $T = 0$, we obtain

$$n_0 = x, \quad n_{1-} = 1 - x, \quad n_{1+} = 0, \quad n_2 = 0. \quad (1)$$

In the generalized tight-binding method, each quasiparticle is characterized not only by the energy but also by the spectral weight determined by the sum of the occupation numbers of the initial and final many-electron terms. Therefore, the doping is accompanied by the redistribution of the spectral weights of the bands $\Omega^{(c)}$ and $\Omega^{(v)}$; that is,

$$F_0 = 1 - x + x = 1, \quad F_1 = 1 - x, \quad (2)$$

Moreover, there arises a new quasiparticle (shown by the solid arrow with the band index 2 in Fig. 4), whose spectral weight is proportional to the doping concentration:

$$\Omega_2 = E_{1,\bar{\sigma}} - E_0, \quad F_2 = x. \quad (3)$$

This is an intragap state induced by *n*-type doping. In the two-hole representation, the level Ω_2 lies higher than the level Ω_0 by the magnitude of the internal molecular field ~J [15]. In the electron representation, the intragap state lies inside the band gap in the vicinity of the bottom of the conduction band. The transition from the top of the valence band to the empty intragap states results in the appearance of the peak separated from the absorption edge E_{g0} in the absorption spectrum by the magnitude of the order of J. Note that J ~ 0.1 eV for cuprates. The intensity of the absorption peak is proportional to the doping concentration, i.e., the concentration of Cu^+ ions and oxygen vacancies.

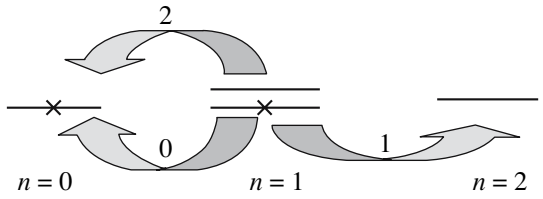

Fig. 4. Schematic diagram illustrating the formation of quasiparticles upon *n*-type doping. The arrow with numeral 2 indicates the intragap state.

Judging from these considerations, we can believe that the absorption bands (found for the samples of nanostructured oxide CuO) in the energy range 1.0–1.3 eV directly below the fundamental absorption edge for the "undoped" copper oxide are associated with the intragap states split from the conduction band. However, the absorption band at 0.6 eV for the nanopowder prepared by the gas-phase method (Fig. 2, curve *2*), in our opinion, is attributed to the defect band lying deep in the band gap.

4. CONCLUSIONS

The quantum confinement of one-electron band states (typical of nanoparticles with free electrons) does not manifest itself for the CuO oxide and other nanoparticles with strong electron correlations, because the main contribution to the formation of quasiparticles is made by the central unit cell and its nearest neighbors. Therefore, the main change in the electronic structure and the optical absorption spectra is associated with the mechanism (specific to systems with strong electron correlations) responsible for the formation of intragap states with the spectral weight proportional to the doping concentration.

Certainly, typical impurities can also be responsible for the deep levels and similar absorption peaks, which are difficult to separate in experiments. In the theory, levels induced by light impurities have a one-electron nature and are associated only with the irregularities and defects of the lattice. In the three-dimensional case, their splitting-out requires a rather deep potential well. The aforementioned intragap states have a many-electron nature and do not necessitate lattice defects. It is sufficient to change only the carrier concentration. Note that this change can be regular; i.e., it can be governed by the variable-valence effect. Actually, both mechanisms operate in the crystal. Note also that a similar red shift in the fundamental absorption edge was observed for nanocrystalline oxide Fe_2O_3 and yttrium iron garnet with a large number of defects generated under quasi-hydrostatic pressure [16, 17]. The appearance of intragap levels with a high density of states in the electronic structure of 3*d* metal nanooxides makes it possible to control the spectral characteristics of these materials and, in particular, to change the effective band gap, i.e., to vary the transparency window. As was demon-

strated in our earlier work [18], this opens up new possibilities for the design of effective materials for selective coatings of solar heaters based on oxide nanomaterials.

ACKNOWLEDGMENTS

This study was supported by the Russian Academy of Sciences within the program "Strong Electron Correlations," the Integration Project of the Siberian Division–Ural Division of the Russian Academy of Sciences (project no. 74), the Federal Agency for Science and Innovation (contract no. 02.434.11.7048), the Russian Foundation for Basic Research (project no. 06-03-32943), and the Branch of General Physics and Astronomy of the Russian Academy of Sciences and the Presidium of the Ural Division of the Russian Academy of Sciences within the program "New Materials and Structures."

REFERENCES

1. Al. L. Éfros and A. L. Éfros, Fiz. Tekh. Poluprovodn. (Leningrad) **16** (7), 1209 (1982) [Sov. Phys. Semicond. **16** (7), 772 (1982)].
2. B. A. Gizhevskiĭ, Yu. P. Sukhorukov, A. S. Moskvin, N. N. Loshkareva, E. V. Mostovshchikova, A. E. Ermakov, E. A. Kozlov, M. A. Uĭmin, and V. S. Gaviko, Zh. Éksp. Teor. Fiz. **129** (2), 336 (2006) [JETP **102** (2), 297 (2006)].
3. V. V. Val'kov and S. G. Ovchinnikov, *Quasiparticles in Strongly Correlated Systems* (Siberian Division, Russian Academy of Sciences, Novosibirsk, 2001) [in Russian].
4. Yu. P. Sukhorukov, N. N. Loshkareva, A. S. Moskvin, and A. A. Samokhvalov, Zh. Éksp. Teor. Fiz. **108**, 1821 (1995) [JETP **81**, 998 (1995)].
5. E. A. Kozlov, E. V. Abakshin, V. I. Tarzhanov, RF Patent No. 2 124 716, 1998.
6. B. A. Gizhevsky, E. A. Kozlov, A. E. Ermakov, N. V. Lukin, S. V. Naumov, A. A. Samokhvalov, V. L. Arbuzov, K. V. Shal'nov, and M. V. Degtyarev, Fiz. Met. Metalloved. **153** (2), 52 (2001) [Phys. Met. Metallogr. **153** (2), 153 (2001)].
7. I. N. Shabanova, A. E. Ermakov, V. A. Trapeznikov, and Ya. S. Shur, Fiz. Met. Metalloved. **38**, 38 (1974).
8. Yu. A. Kotov and N. A. Yavorskiĭ, Fiz. Khim. Obrab. Mater., No. 4, 24 (1978).
9. A. P. Druzhkov, B. A. Gizhevskii, V. L. Arbuzov, E. A. Kozlov, K. V. Shalnov, and D. A. Perminov, J. Phys.: Condens. Matter **14**, 7981 (2002).
10. B. A. Gizhevskiĭ, V. R. Galakhov, D. A. Zatsepin, L. V. Elokhina, T. A. Belykh, E. A. Kozlov, S. V. Naumov, V. L. Arbuzov, K. V. Shal'nov, and M. Neumann, Fiz. Tverd. Tela (St. Petersburg) **44** (7), 1318 (2002) [Phys. Solid State **44** (7), 1380 (2002)].
11. A. Ye. Yermakov, M. A. Uimin, V. R. Galakhov, A. A. Mysik, O. V. Koryakova, V. G. Kharchuk, V. A. Vykhodetz, V. S. Gaviko, K. Kuepper, S. Robin, and M. Neumann, J. Metastable Nanocryst. Mater. **24–25**, 43 (2005).
12. Yu. P. Sukhorukov, N. N. Loshkareva, A. S. Moskvin, V. L. Arbuzov, and S. V. Naumov, Pis'ma Zh. Tekh. Fiz. **24** (2), 7 (1998) [Tech. Phys. Lett. **24** (2), 127 (1998)].
13. N. N. Loshkareva, Yu. P. Sukhorukov, B. A. Gizhevskii, A. S. Moskvin, T. A. Belykh, S. V. Naumov, and A. A. Samokhvalov, Fiz. Tverd. Tela (St. Petersburg) **40** (3), 419 (1998) [Phys. Solid State **40** (3), 383 (1998)].
14. V. A. Gavrichkov and S. G. Ovchinnikov, Zh. Éksp. Teor. Fiz. **125** (3), 630 (2004) [JETP **98** (3), 556 (2004)].
15. S. G. Ovchinnikov, A. A. Borisov, V. A. Gavrichkov, and M. M. Korshunov, J. Phys.: Condens. Matter **16**, L93 (2004).
16. J. K. Vassiliou, V. Mehrota, M. W. Russell, E. P. Giannelis, R. D. McMichael, R. D. Shull, and R. F. Ziolo, J. Appl. Phys. **73**, 5109 (1993).
17. A. G. Gavriliuk, V. V. Struzhkin, I. S. Lyubutin, and I. A. Trojan, Pis'ma Zh. Éksp. Teor. Fiz. **82** (9), 682 (2005) [JETP Lett. **82** (9), 603 (2005)].
18. Yu. P. Sukhorukov, B. A. Gizhevskii, E. V. Mostovshchikova, A. E. Ermakov, S. N. Tugushev, and E. A. Kozlov, Pis'ma Zh. Tekh. Fiz. **32** (3), 81 (2006) [Tech. Phys. Lett. **32** (2), 132 (2006)].

Translated by O. Borovik-Romanova